# 'UNIVERSAL' DYNAMICS IN THE WAKE OF AN OSCILLATING CYLINDER AT LOW REYNOLDS NUMBERS

**D. J. Olinger and K. R. Sreenivasan**
Mason Laboratory, Yale University
New Haven, Connecticut

## ABSTRACT

We present experimental observations in the wake of an oscillating circular cylinder at low Reynolds numbers. The fluid system is one in which a limit cycle (corresponding to the natural vortex shedding) is modulated at a second frequency (due to the cylinder oscillation) generating in phase space a flow on a torus. At rational values of the frequency ratio, the system displays Arnold tongues due to phase locking, leading to a behavior approximating the devil's staircase along the critical line. Associated with quasiperiodic transition at the golden mean frequency ratio, spectral peaks appear at various Fibonacci sequences. These as well as the 'singularity spectrum' of the Poincare section of the attractor at the critical golden mean point are largely similar to the universal characteristics of the sine circle map, the observed departures being within experimental uncertainties.

## NOMENCLATURE

| | |
|---|---|
| $a$ | Cylinder oscillation amplitude |
| $D$ | Cylinder diameter |
| $D_0$ | Fractal dimension of the support |
| $D_q$ | Generalized dimensions |
| $f_e$ | Cylinder oscillation frequency |
| $f_0$ | Natural vortex shedding frequency |
| $f_0'$ | Shifted vortex shedding frequency |

$f(\alpha)$ Fractal dimension of iso-$\alpha$ surface

K Non-linearity parameter

Re Reynolds number

$\alpha$ Local probability scaling index

$\alpha_{GM}, \delta$ Scaling parameters for critical golden mean point

$\theta$ Radian measure on circle map

$\sigma_G$ Dressed winding number at critical golden mean point

$\Omega$ Bare winding number, $f_e/f_0$

$\omega$ Dressed winding number, $f_e/f_0'$

## 1. Introduction

An outstanding problem in fluid mechanics is the understanding of the manner in which a fluid flow changes its characteristics from a steady laminar state to a fully turbulent one. By a careful combination of experiment and theory in several prototypical flows, a reasonable picture of flow dynamics in the early stages of this development is slowly emerging. Quite distinct in spirit are the attempts to hypothesize and demonstrate some universality in these stages. Landau [1] argued that turbulence is the asymptotic state of a flow that repeatedly undergoes a supercritical Hopf bifucation, yielding a combination of increasingly higher order quasiperiodicities. Recent work in nonlinear dynamics of systems with small degrees of freedom has provided an alternative point of view according to which a complex state termed 'chaos' (not necessarily turbulence) can evolve after a few bifurcations. Two specific points of interest in the recent work are the demonstration that chaos, or temporal complexity, does not require many degrees of freedom, and that there are some 'universal' features accompanying such transition; the implication in this last notion is primarily that there are some features of such transition that transcend the governing equations of motion, but are controlled essentially by the topological structure of the attractor in phase space.

In low-dimensional dynamical systems, detailed predictions have been made for these 'universal' features of transition to chaos by the period-doubling [2,3], as well as the quasiperiodic [4-7] routes. We are interested here especially in the quasiperiodic route to chaos. Theoretical studies of transition from quasiperiodicity to chaos follow the well-known Ruelle-Takens-Newhouse [8,9] route to chaos in which, first, a stable flow undergoes a Hopf bifurcation to a limit cycle as some control parameter is increased; loss of stability of this new state leads to quasiperiodic motion with two incommensurate frequencies. The next bifurcation would yield a quasiperiodic motion with three frequencies: it has been shown [9] that even a weak nonlinear coupling among these three frequencies is likely to result in chaos. It is important to note that the above scenario gives us no information on the possible universality properties of this route to chaos, and indeed no universality has been noted in several physical systems which follow this route, unlike those in which period-doubling occurs. This is

inherently due to the fact two control parameters are relevant to the quasiperiodic route. As we shall see, there is in this case the additional possibility that mode-locked states interrupt transition to chaos, and that, to observe universal behavior, it is necessary to control both parameters in such a way as to avoid mode-locked states.

Before we describe the nature of this universality in quantitative terms, a brief qualitative description is useful. We refer to a physical system containing two competing non-linearly coupled oscillators, one of which is a natural oscillation of the system at frequency $f_0$ (say), while the frequency ($f_e$) and amplitude (K) of the second oscillator is externally imposed on the system. The amplitude of the oscillation $f_0$ is imposed naturally so that the amplitude of the second oscillator is analogous to the non-linear coupling in the system. We expect that in the presence of the non-linear coupling the natural system oscillation frequency will shift from its uncoupled value of $f_0$ to some new frequency $f_0'$. Following the terminology common in the dynamical systems literature, we define the ratios $\Omega = f_e/f_0$ and $\omega = f_e/f_0'$ as the bare and dressed winding numbers respectively. When the amplitude of non-linear coupling between the two oscillators is small we can expect two distinct possible states to appear – the quasiperiodic state in which the ratio of the frequencies or dressed winding number is an irrational, and the mode-locked state in which the dressed winding number is a rational number p/q. Within a mode-locked state, if one adjusts $\Omega$ or K within a certain range, the second oscillator adjusts itself so that the winding number $\omega$ remains at the rational number p/q. A convenient way of characterizing these two states is in terms of the non-linear coupling amplitude *vs* bare winding number plane (K *vs* $\Omega$) in which the mode-locked states appear as the so-called Arnold tongues, whose width increases as K increases; an Arnold tongue exists for every rational number p/q. The width of each tongue at a fixed amplitude K rapidly decreases as the denominator q increases. The tongues themselves are ordered through a Farey composition which will be explained in more detail in later sections.

Because the Arnold tongues widen as K increases they eventually overlap at some critical amplitude. Above this critical amplitude chaotic states are permissible. Chaos arises simply because the system continuously shifts between one of several mode-locked tongues. The transition to chaos is studied by fixing the dressed winding number to some irrational value, and by increasing K towards and through the critical amplitude line; universal predictions of this transition are observed when K is precisely at the critical amplitude. It must be emphasized that since mode locking is expected to occur for all rational values of the winding number, universal behavior will occur only when K is increased along an irrational value of $\omega$, the most important one being the 'golden mean' to be described below.

To study the K-$\Omega$ space it is necessary to control the frequency and amplitude of one oscillator independent of the second. This is in direct contrast to a system in which the amplitude and frequency of both oscillators is allowed to shift, as in a system where both frequencies are flow-generated. In this latter case, a variation in amplitude of one of the oscillators may cause both frequencies to shift due to feedback between the two oscillators. In a proper experiment, the coupling should be one-directional, that is, the externally imposed oscillator should act on the internal one but not *vice versa*; in particular, there should be no shift in the frequency of the second oscillator as its amplitude is varied. It should be obvious that to explore the K-$\Omega$ plane one must externally control both parameters, K and $\Omega$, in contrast to the period doubling and intermittency cases where only one control parameter characterizes the transition scenario. This makes experimental studies of quasiperiodic transition inherently more difficult.

Several experiments in closed flow, small aspect ratio, Rayleigh Benard convection systems [10-15] have gone a long way in establishing the validity of these predictions to continuous flow systems. However, experiments in open flow systems (those with imposed unidirectional main flow) with little or no confinement have been

quite rare [16-20], and inconclusive on occasion [17]. The best case showing evidence of universal features of nonlinear dynamics is the flow behind circular cylinders [16]. Here, we seek to experimentally study the universal transition from quasiperiodicity to chaos in the flow behind an oscillating cylinder at low Reynolds numbers and show that the system exhibits many quantitative features of universality.

Specifically, in the wake of an oscillating cylinder, the internal oscillator is the natural vortex shedding mode characterized by the well known Karman vortex street, while the second oscillator is externally imposed by forcing the cylinder in its fundamental resonant mode transverse to the flow at some desired frequency and amplitude. One then studies the coupled wake response as a function of these two parameters by placing a hot wire probe some distance downstream of the cylinder and measuring the streamwise velocity fluctuations. The experimental data is analyzed by obtaining power spectra, phase plots and Poincare sections of the dynamical trajectory.

The model dynamical system for which the theory is well-developed is the so-called circle map, which is a map of the circle on to itself. The relevance of this map to the system described above can be cast in the following language. A system with two competing frequencies describes in phase space a trajectory on a torus. If this torus is cut by a Poincare plane, the trajectory intersects the plane in points topologically equivalent to a circle. As discussed previously, two behaviors are possible in a system with two competing frequencies, namely mode-locking and quasiperiodicity. In a mode-locked state, the orbit on the torus is a closed one-dimensional curve. If quasiperiodicity exists the orbit does not close, and the surface of the torus is filled completely resulting in a surface. Much work has been done, utilizing both numerical studies and renormalization group techniques, towards the theoretical understanding of circle maps [4-7]. We review these features in Section 2, while in Section 3 we provide a rationale for expecting them to be relevant to low Reynolds number flow past circular cylinders. We describe the experimental set-up in Section 4, and the results in Section 5, where a comparison with circle map predictions is made. Some conclusions are presented in Section 6. We note that this manuscript represents an expansion of work presented previously in Ref. 20. Figures 3,5,6,12,15 and 20 are taken from this work.

## 2. THE THEORY OF QUASIPERIODIC TRANSITION TO CHAOS

### 2.1 General Concepts

Before proceeding further, it is useful to review briefly the concepts of flow in phase space and Poincare sections. To construct an N-dimensional phase space flow diagram one plots, with time t as the parameter, N independent variables $u_i(t)$, $i = 1, 2,...,N$, where $u_i(t)$ represent any N dynamic variables, for example velocity traces at N different points in the wake. For example, for N=3 one would plot $u_1(t)$ *vs* $u_2(t)$ *vs* $u_3(t)$ for all t. Obviously measurement of N independent variables is a difficult if not hopeless task, but embedding theorems like those of Takens [21] (see also Eckmann & Ruelle [22]) justify the use of a single measured variable. From one measured local velocity component u(t), for example, one constructs a d-dimensional diagram from the vectors $[u(t_i), u(t_i + \tau),....., u(t_i+(d-1)\tau)]$, $i = 1,....., N(large)$. The time delay $\tau$ must be so chosen that each of the components of the vector so constructed are independent, but its precise value in a certain wide range seems to be immaterial. According to embedding theorems, phase diagrams constructed in this way will have essentially the same properties as the one with N independent variables, if $d > 2N + 1$. A flow with a single periodicity will trace out a closed one-dimensional curve in phase space. Upon bifurcation to a quasiperiodic state, the phase diagram will undergo transition to a two-torus in phase space which is simply the product of the phase spaces of each the two oscillators in the system. Transition to chaos results in a deformation of this torus, and the phase portrait becomes a strange attractor. Thus one

studies the dynamical behavior of a quasiperiodic flow by considering different types of orbits on the torus.

The dimension of the problem can be reduced by one *via* the Poincare section of the attractor, with this operation preserving the essential dynamics. The Poincare section is merely a cross-section of the torus formed by cutting it with a plane. The intersection of the orbits on the two-torus and the Poincare plane is then topologically equivalent to a circle. If the orbit on the torus is mode-locked with dressed winding number p/q, the Poincare section will take the form of a set of q discrete points on a circle. If the flow is quasiperiodic (irrational dressed winding number) the Poincare section will be densely filled, and look topologically equivalent to a continuous circle. Experiemntally, one forms a Poincare section by sampling the continuous time trace which winds the torus at the frequency of either of the two dominant frequencies in the flow. The dynamics of the system is then reduced to a study of its Poincare section.

## 2.2 Circle Map: Sub-Critical Behavior

The next concept of interest is the circle map which is a functional relationship between the angular coordinate at the n-th crossing $\theta_n$ and the (n+1)-th crossing $\theta_{n+1}$ of the Poincare section. The map which has most often been studied is the sine circle map which takes the form

$$\theta_{n+1} = \theta_n + \Omega - (K/2\pi)\sin(2\pi\theta_n), \qquad (1)$$

where $\theta$ is the angular coordinate on the Poincare section, $\Omega$ is the bare winding number and K is a non-linearity parameter as previously discussed. We shall see later that the specific form of this map within a certain wider class is unimportant. The map is utilized by setting $0 < \Omega < 1$ and $K > 0$ and obtaining the iterates $\theta_n$. From our previous discussion we see that $\omega$, the dressed winding number, is not obtainable from a casual study of the map. The dressed winding number is defined as

$$\omega = \lim_{n\to\infty} [(\theta_n - \theta_0)/n]. \qquad (2)$$

When K=0, we see that $\Omega = \omega$, but $\Omega \neq \omega$ for $K > 0$. The dressed winding number represents the average shift per iteration in the sine circle map in the presence of non-linear coupling.

Analogies between the circle map and the Poincare sections in a system with two competing frequencies must now be obvious. A circle map models the Poincare section of a two frequency quasiperiodic flow in phase space before, during and at the transition to chaos. The circle map is mode-locked when $\omega$ is a rational p/q in which case there will only be q distinct $\theta_n$ in the iteration; that is, $\theta_{n+q} = \theta_n + p$. In a quasiperiodic case where $\omega$ is irrational, the $\theta_n$ will never repeat itself and the Poincare section will be densely filled. Studying the global properties of the K-$\Omega$ plane for the circle map yield the picture described in Section 1. Arnold tongues occurring at all rational p/q increase in width as K increases, so that for small K the mode-locked behavior is rare and quasiperiodicity predominant. This behavior is reversed at larger K. The overlap of various mode-locked tongues occurring at K=1 represents transition to chaos. The Arnold tongues are ordered through the Farey composition constructed according to the following procedure. Given two parent tongues corresponding to the rationals $p_1/q_1$ and $p_2/q_2$, one defines their daughter corresponding to $(p_1+p_2)/(q_1+q_2)$. The daughter's p/q lies between the two respective parents and has the smallest denominator of any rational p/q between the two parents. As mentioned previously, the widths of the tongues decrease rapidly with increasing q, and so the daughter tongue is always smaller in width than those of its two parents.

## 2.3 Circle Map: Critical Behavior

We now turn to the behavior of the map at K=1 where transition to chaos occurs. Along the critical line the set of all mode-locked $\Omega$ form a Cantor-like set. Its complement has a fractal dimension $D_0$ which has been calculated numerically to be 0.87. (In general, the fractal dimension contains scaling information on the number N of d-dimensional boxes sized r required to cover an object embedded in the d-dimensional space and is defined by

$$N \sim r^{-D_0}. \tag{3}$$

The fractal dimension is integer for Euclidean objects, but in general a fraction for fractal objects.) These mode-locked $\Omega$ also form a devil's staircase structure when plotted in the form $\omega$ *vs* $\Omega$. (A precise discussion of the staircase structure will be delayed until Section 5.) The fractal dimension of the staircase structure on the critical line is a universal property of all circle maps with the only restriction being that the non-linear one-dimensional map has a cubic inflection point. We need not therefore study the sine circle map specifically, any map in this wider class being adequate. Thus a different circle map may yield a staircase structure different in detail from the sine circle map, but the global properties such as the fractal dimension will be the same. Experimentally, universality implies that various universal properties of the quasiperiodic route to chaos may be found in a wide range of different physical systems. This universality is important as this gives a clue to the map representative of the experimental system. As remarked already, universal properties in various systems undergoing transition to chaos *via* the quasiperiodic route are less commonly observed, and this work is aimed at filling some of this gap.

Returning now to the universal properties in the transition to chaos at some irrational $\omega$ as K approaches the critical line, we note that an irrational $\omega$ can never be attained to infinite precision. However, an irrational $\omega$ can be approximated by a sequence of rational numbers to which it converges. We do this by truncating the continued fraction representation of an irrational

$$\omega = \cfrac{1}{n_1 + \cfrac{1}{n_2 + \cfrac{1}{n_3 + \cdots}}} \tag{4}$$

denoted by $[n_1,n_2,n_3,...]$. We focus on the golden mean represented by $\omega = \sigma_G = [1,1,1,1,...] = (\sqrt{5} - 1)/2$, also represented using a Fibonacci sequence defined as $F_{i+2} = F_i + F_{i+1}$ where $F_0 = 0$ and $F_1 = 1$; $F_i / F_{i+1}$ approaches $\sigma_G$ for large i. The critical golden mean point ($\omega = \sigma_G$, K=1) has been studied most extensively because $\sigma_G$ is the irrational number least well approximated by rationals (since the continued fraction representation is made up of 1's converges the slowest), the implication being that the transition point K=1 in the circle map is the farthest away from any mode-locked tongues at the critical line. Experimentally this means that it should be the easiest point at which to realize universal transition to chaos can be realized while avoiding mode-locking. The importance of this condition has been discussed previously.

Universality in the transition from quasiperiodicity to chaos at the critical golden mean point in circle maps is best observed in a scaled power spectrum. Following Rand et al. [7] we introduce a time dependence into the iterates of the map with the following construction

$$u(t_j) = \theta_j - j\,\sigma_G, \qquad j = 1, 2, 3, ..., \infty \tag{5}$$

and take a Fourier spectrum of $u(t_j)$. The circle map predicts a self-similar scaled power spectrum when power is scaled by frequency squared ($P(f)/f^2$) plotted versus log of the frequency f. The power spectrum is divided into bands by peaks at all powers of $\sigma_G$. Due to the mathematical nature of the golden mean these are nothing more than the principal difference frequencies $f/f_0' = |m\sigma_G - n|$, where $|\ |$ denotes absolute value and the integers m and n are such that m>n. These peaks are commonly designated as generation 1 peaks and are at constant amplitude for all powers of $\sigma_G$. We also see that this generation can be created using from a Fibonacci sequence (0,1,1,2,3,5,8,13,...) where the values in this sequence are used as m and n in the above difference equation; for example, m = 2, n = 1 results in $\sigma_G^3$. Other generations are produced using different Fibonacci seeds, for example generation 2 by the sequence (0,2,2,4,6,10,...), generation 3 by (1,3,4, 7,11,...), etc. Peaks within each generation are of constant peak amplitude, but this amplitude is different from generation to generation.

## 2.4 Generalized Dimensions and the Singularity Spectrum

The iterates $\theta_n$ for the sine circle map at the critical golden mean point are non-uniformly distributed on the set $0 < \theta_n < 1$. There are regions where the iterates are highly concentrated just as there are highly rarefied regions. In situations such as this, one is often interested in how often a given region of the attractor (or the Poincare section) is visited. In general, one can describe such events by dividing the attractor into pieces with an index i (1 to N), the size of each piece being given by r. The frequency $N_i$ with which the $i^{th}$ piece is visited can be defined by $p_i = \lim_{N\to\infty}(N_i/N)$. One describes this probability by defining a local index $\alpha(i)$ *via* $p_i = r^{\alpha(i)}$. Typically for small r, $\alpha(i)$ takes on continuous values in the range $\alpha_{min}$ and $\alpha_{max}$. We now use the fact that the fractal attractor can in general be described as an interwoven set of homogeneous fractals [23-25].

Let $f(\alpha)$ be the fractal dimension of the homogeneous fractal set corresponding to a given $\alpha$. (For convenience, we have eliminated the index i on $\alpha$.) This means that for an attractor divided into pieces of size r, the number of times $n(\alpha,r)$ that $\alpha$ takes a value between $\alpha$ and $\alpha+d\alpha$ is given by $n(\alpha,r) = d\alpha\rho(\alpha)r^{-f(\alpha)}$. Here, $\rho(\alpha)$ is some density. The intuitive meaning of $\alpha_{min}$ is that it describes the most concentrated regions of the set, while $\alpha_{max}$ describes the most rarefied regions. Typically $f(\alpha_{max}) = f(\alpha_{min}) = 0$, and $f(\alpha)$ is such that $0 < f(\alpha) < D_0$, where $D_0$ is the fractal dimension of the support of the original set (in this case the attractor or its Poincare section). The function $f(\alpha)$, also called the multifractal spectrum, is a universal property of the trajectory of the iterates at the critical golden mean point for circle maps. One first determines the quantity $\Gamma(q,r) = \Sigma p_i^q$ taking the summation over all boxes or pieces i of length r. This quantity scales as $\Gamma(q,r) = r^{(q-1)D_q}$ where the $D_q$ are the so called generalized dimensions [22,23]. For q=0 the above formulation yields simply the fractal dimension $D_0$. One can then determine the $D_q$'s over a range of q values to yield a $D_q$ *vs* q curve which summarizes the scaling properties of cumulants of the probability distribution on the set. In practice one divides the attractor into boxes of equal size r and then plots $\log(\Gamma(q,r))/(q-1)$ *vs* $\log(r)$ for various sizes r whose linear slope yields $D_q$. The $D_q$ *vs* q curve for the critical golden mean point is also universal. Using the Legendre transformation it is possible to directly convert the $D_q$ *vs* q curve into the $f(\alpha)$ *vs* $\alpha$ curve *via* the pair of formulas [23]

$$\alpha = d/dq\ ((q-1)D_q) \tag{6}$$

$$f(\alpha) = q\alpha - (q-1)D_q \tag{7}$$

Thus by determining the $D_q$'s we can easily obtain the $f(\alpha)$ *vs* $\alpha$ curve. Both this and the $D_q$ curve will be presented in Section 5 along with experimental results.

Other universal properties in the transition to chaos at the critical golden mean point can be obtained by looking at scaling indices analogous to those found in the period doubling route. Strong evidence for scaling in the circle map has been shown by several groups. For some value of K, denote by $\Omega_i(K)$ the value of $\Omega$ for which a cycle with dressed winding number $\omega_i$ passes through $\theta=0$. Then $\delta$ is defined as a scaling index for the convergence of the $\Omega_i(K)$. In general, following Jensen et al. [26], the $\Omega_i$ (K) are interpreted as the width of the various mode-locked tongues at some K for each $\omega_i$ in the Fibonacci sequence converging to the $\omega$ under study. That is,

$$\delta = \lim_{i\to\infty}[(\Omega_{i+1} - \Omega_i) / (\Omega_i - \Omega_{i-1})] \qquad (8)$$

The value for $\delta$ for K=1 and $\omega = \sigma_G$ is equal to –2.83362.. A second scaling index is defined by

$$\alpha_{GM} = \lim_{i\to\infty} [d_i/d_{i+1}] \qquad (9)$$

where $d_i$ represents the distance between $\theta=0$ and the closest element on the $q_i$ cycle closest to it. This says that the distances around $\theta=0$ in the circle map scale down by a universal factor $\alpha_{GM}$ when the iterations on the trajectory is truncated at two consecutive Fibonacci numbers. The value of $\alpha_{GM}$ at the critical golden mean point is equal to 1.28857.... More will be said in Section 5 concerning the experimental determination of these indices.

## 3. VORTEX SHEDDING BEHIND CIRCULAR CYLINDERS

We now turn to a review of the relevant features of low Reynolds number flow behind circular cylinders. Briefly, with increasing Reynolds number, the flow behind a stationary circular cylinder in a low turbulence wind tunnel first undergoes a Hopf bifurcation [27] from the steady state to a periodic state corresponding to the familiar vortex shedding mode. The flow in this state is characterized by the natural vortex shedding frequency $f_0$. We have shown in [27] that the post-critical state can be modelled by the Landau equation, and determined the Landau constants. For cylinder aspect ratio (that is, the length to diameter ratio) exceeding about 60, details appear independent of the aspect ratio, and the critical Reynolds number $Re_{critical}$ (based on the cylinder diameter D, the oncoming free stream velocity, and the kinematic viscosity of the working fluid, namely air) is about 46. The relevant measurements were of the transient type.

As shown by Sreenivasan [16], with further increase in Reynolds number, the stability of this state is lost in favor of quasiperiodic state with two incommensurate frequencies in the Reynolds number range, $18 < (Re - Re_{critical}) < 30$. Further increase in the Reynolds number leads to a chaotic state. These transitions seem to follow the well known quasiperiodic route to chaos. As the Reynolds number is further increased, reordering to a state with three incommensurate frequencies was observed on occasions, and so deviations from this scenario appear to exist. The relevance of these facts to our present discussion is obvious given that we seek to study the universal transition from quasiperiodicity to chaos, although we will have no occasion to use them directly. Van Atta & Gharib [28] have argued that the observed quasiperiodic and chaotic states are due to cylinder vibrations, and are not a part of the dynamics of the wake behind the stationary cylinder. We delay discussion of this at this time (because it is not directly relevant to us here), but do note that Van Atta & Gharib seem to have observed lock-in states. In fig. 4 of their paper we note a p/q = 1/5 lock-in state in which the vortex shedding frequency and natural cylinder oscillation frequency are in a rational ratio. However, we note that they use a freely

vibrating cylinder and did not control cylinder oscillation amplitude independently. The freely vibrating cylinder allows for vibration in higher order modes, the 5th harmonic in the case of the example just cited. In the present experiments, it was always ensured that the cylinder vibrated in the fundamental mode. The lock-in observed by Van Atta & Gharib occurs because the wake forces the cylinder to oscillate in the 5th harmonic mode and then locks on to the frequency associated with this mode. In our study, we monitor and accurately control the amplitude, mode shape and the frequency of oscillation, this being the key to the success of the experiment.

Before presenting the experimental results, we briefly discuss additional motivation for believing that the oscillating cylinder wake is an excellent system to study. Since Koopman [29] it has been widely known that cylinder oscillations can have a dramatic effect on the wake structure behind a circular cylinder. The most dramatic of these effects correspond to the case when the natural vortex shedding frequency "locks on" to the cylinder oscillation frequency; this occurs when the ratio of the two frequencies is close to unity. From our previous discussions we note that this is the 1/1 lock-in ($p = q = 1$) where $\Omega$ is set near 1. This lock-in range increases in width as the amplitude of the cylinder oscillation increases and hence is qualitatively similar to Arnold tongues of the circle map. Our search for additional phase locked tongues at other rational $\omega$'s constitutes a generalization of this work within the framework of dynamical systems. Additionally, work by Stansby [30] and Ongoren & Rockwell [31] seems to show evidence of other p/q mode-lockings, but none of this work makes a connection to dynamical systems. In particular, Ref. [31] notes a 1/1.5 lock-in which is similar to the 2/3 lock-in state we will demonstrate shortly. Finally, analogies can be drawn between the present flow and other fluid systems (most notably the Rayleigh-Benard convection cell) which have exhibited quantitative experimental results reminiscent of circle maps. In the small aspect ratio cells with only a few convection rolls present, the time averaged spatial structure of the flow is fixed, yielding a time dependent dissipative non-linear system with only a few degrees of freedom. Establishing similarities in a very different, and inherently more complex, type of fluid system has significance beyond the immediate. It seems possible to do this. For example, Sreenivasan et al. [27] have shown that many features of the post-critical state of vortex shedding can be described by a purely temporal model, and that only a few relevant degrees of freedom exist if one is not too far above the critical Reynolds number. We recognize that our review of vortex shedding behind stationary and oscillating cylinders has been limited to matters pertinent to the present discussion. For more detailed information we refer the interested reader to the excellent review articles available [32,33].

## 4. EXPERIMENTAL ARRANGEMENT

Figure 1 shows the experimental set-up employed in this study. For the present measurements, the Reynolds number was held fixed at some value between 54 and 60, equivalently $8 < (Re - Re_{critical}) < 14$. From previous discussion it is obvious that we wish to create a system with two competing frequencies which we accomplish by imposing a second external frequency. In section 3, the possibility of naturally occurring two frequency quasiperiodicities was noted, and hence we choose to operate in this Reynolds number range above $Re_{critical}$. The wind tunnel used in this study is of suction type with double contractions upstream of the 15 cm square test section. Honeycomb and several damping screens are utilized to ensure a clean, laminar freestream flow. The freestream turbulence level at flow velocities of interest in this study is approximately 0.1%. The working fluid is air. Stainless steel wires 0.03 to 0.09 cm in diameter whose geometric uniformity was checked under a microscope were used as cylinders. The cylinder was stretched through the test section using a tensioning device placed outside the test section with which one could change the

resonant frequency of the cylinder. The active length of the cylinder was 15 cm yielding aspect ratios (cylinder diameter/length) in the range 160 to 500. The actual cylinder length between the tensioning supports was approximately 5 times the active length. This ensured that when the cylinder vibrated the variation in cylinder oscillation amplitude across the active length of the cylinder was small. This variation was measured experimentally and found to be less than 3% of the cylinder diameter.

A modulation is imposed by externally oscillating the cylinder transversely at a frequency $f_e$. The cylinder oscillation at the desired frequency is accomplished by passing a sinusoidally alternating current from a signal generator through the cylinder placed in a properly aligned magnetic field. The signal generator is tuned very carefully to the wire's resonant frequency obtained by simply adjusting the tension and plucking the wire. This ensures that the oscillation of the cylinder is always in its first mode. The alternating current passing through the wire may of course result in heating of the wire, thus affecting the flow dynamics. This was thoroughly investigated; as shown in figure 2, for currents required to generate sufficient oscillation amplitudes, there was little effect on the power spectrum of a hot wire placed in the cylinder wake. The natural vortex shedding frequency shifted by less than 0.5% when the current is removed. Note that these two conditions represent the two extremes in cylinder temperature that might be encountered during an experiment. We should note that the amplitude of cylinder oscillations was controlled by the strength of the magnetic field and not by varying the current amplitude, so that the cylinder current was constant throughout the experiment whether the cylinder was oscillating or stationary. We recognize that this does not imply constant cylinder temperature as the heat transfer rate from the cylinder will depend on the values of a/D, $\Omega$, and $\omega$. These facts were also reconfirmed by completely eliminating the current from the system, using a non-heated cylinder which was mechanically plucked to achieve the oscillation. While the cylinder oscillation amplitude is hard to control using this latter method, we did note identical phenomenon (mode-locking, etc.) as with our standard method of oscillation. Electromagnets of strength on the order of 10 Gauss were used to create the magnetic field. The magnetic field could be varied to change cylinder oscillation amplitude or turned off completely for the stationary cylinder case. It should be noted that when studying the stationary case to obtain $f_0$ the cylinder was also damped with foam rubber at either side of the test section to ensure that no residual magnetic field could oscillate the cylinder.

The cylinder oscillation amplitude was measured using a MTI Fotonic Sensor, placed at the tunnel test section wall outside the flow. This probe measures reflected light off the cylinder, the intensity of the electric field of the reflected light being linear with the distance of the probe from the cylinder. Thus an analog signal of the cylinder oscillations is obtained. This probe has a resolution down to 1 microinch. A hot-wire (5 μm dia., 0.6 mm long) placed approximately 15D downstream of the cylinder, 0.5D to one side of its resting position, monitored the wake velocity in the streamwise direction. The hot wire was placed at the tunnel centerline unless otherwise noted. The hot wire signal was amplified, digitized by a twelve-bit analog-to-digital converter and stored in a computer (MASSCOMP 5500) for later analysis. A HP3561A spectrum analyzer was used for real time analysis of Fourier spectrum. All power spectra presented are averaged over at least ten spectral samples. Cylinder oscillation frequency and amplitude were varied over a range of 26-100% of $f_0$ and 0-200% of cylinder diameter. Both the vortex shedding and modulation frequencies were steady to ±2 parts in $10^4$. This stability was noted by studying power spectra of the appropriate time signals using the spectrum analyzer with frequency resolution on the order of ±1 part in $10^5$ over time scales 2 order of magnitudes larger than those used in obtaining spectral averages. For all power spectra presented the frequency resolution of the spectrum analyzer was of the order of ±1 part in $10^3$. The cylinder oscillation amplitude was measured by reading a peak-to-peak voltage of the fiber optic

probe output from an oscilloscope screen. This amplitude could be read to ±3% within which the amplitude was steady over time scales much longer than those used for spectral averaging.

The system considered here meets all previously discussed requirements of a system with two competing frequencies. The nomenclature $f_e$, $f_o$, $\Omega$, and $\omega$ maintain their previous meaning; note that $f_o'$ represents the frequency of the wake oscillations in the presence of the cylinder oscillation. The normalized cylinder oscillation amplitude (a/D) is analagous to the non-linearity parameter K in our previous discussions. We wish to point out that our system does not have one-directional coupling in its strictest sense in that the wake can affect the amplitude, though not the frequency, of the cylinder oscillations. For example, if the flow is completely turned off the amplitude of the cylinder amplitude shifts from its value with flow on, that is, there is some feedback from the wake. Other investigators [13] have utilized a very strict definition of one-directional coupling implying that there can be no feedback from the natural to the external oscillator. Our definition implies that feedback is allowable as long as it does not compromise our ability to map the a/D *vs* $\Omega$ plane or to study an arbitrary irrational winding number. Since the cylinder oscillation amplitude and frequency are imposed externally and controlled accurately, so that $f_e$ does not shift as a/D varies, we meet this requirement completely satisfactorily. We see in the next section that this is indeed the case.

## 5. EXPERIMENTAL RESULTS

### 5.1 Sub-Critical Behavior (Mode-Locking)

Figure 3 highlights the effect of cylinder oscillations on the wake by showing the power spectra of streamwise velocity and cylinder oscillation. Figure 3a shows the natural vortex shedding wake spectrum with no cylinder oscillation. Figure 3b is a spectrum of the cylinder oscillations taken from the fiber optic probe output. In fig. 3c we see the coupled wake spectrum in the presence of cylinder oscillations. We note the shift of $f_o$ to $f_o'$ between figs. 3a and 3c, and the complete suppression of $f_o$ in favor of $f_o'$ in fig. 3c. The sharpness (> 5 orders of magnitude above background noise levels) of all the principal peaks in fig. 3c (linear combinations of $f_e$ and $f_o'$) is remarkable. In this case $\Omega = 0.577$, while $\omega = 5/9 = 0.55555..$, and a/D = 0.15. Figure 4 shows the velocity power spectra for the 1/3 lock-in case; for convenience, the cylinder oscillation spectrum is not shown here. From several such spectra one can create the a/D *vs* $\Omega$ plot showing Arnold tongues (fig. 5) described earlier. Symbols represent points on the plane where data have been stored; boundaries of the tongues shown were determined from a larger set of points. The dressed winding numbers in these tongues correspond to rationals constructed according to Farey arithmetic although, due to limitations in experimental control, no more than 30 such tongues have been identified. In accordance with predictions for the circle map, these tongues increase in width as the non-linearity parameter (a/D) increases. The 1/1 tongue is in close agreement with the previously mentioned 'lock-in' region near $f_o$. The dashed line represents the experimentally determined 'best fit' critical line found by determining for various $\Omega$ the a/D level at which the fractal dimension along the critical line was equal to 0.87 appropriate to the circle map. It was also verified that transition to chaos, as evidenced by spectral broadening, did indeed occur across the critical line. The dimension $D_o$ was computed using the relation[10]

$$\sum_i (S_i / S)^{D_o} = 1 \qquad (10)$$

where S is the distance between two parent tongues and the $S_i$'s are the distances

between a daughter tongue and each of its parents. This equation is derived simply from the previously noted scaling law $\Sigma p_i^q = r^{(q-1)D_q}$ for q=0, and can be shown to be true for the Cantor-set construction. All possible parent-daughter combinations of the tongues shown in figs. 5 and 6 were used. The upturn in the critical line near $\Omega$ = 0.3 is not understood at present, but we note that this must be related to the receptivity of the wake to external oscillations; other investigators [10] have found a non-constant level of non-linearity parameter along their critical line. The symbol (□) represents the critical golden mean point for which observation were made of the scaled power spectra shown later. The symbol (▲) represents the 5/9 lock-in shown in detail in fig. 3. While the work described above is limited to a small Reynolds number range it should be pointed out that we have conducted preliminary studies at higher Reynolds numbers of approximately 80 and seen the same qualitative behavior in the a/D *vs* $\Omega$ plane

In fig. 6 we highlight the fine structure of the phase diagram in a region just below the 1/3 tongue. Typical uncertainties in frequency and amplitude are shown on the boundary of the 3/10 lock-in tongue. Again we note the increase in width as a/D increases. The fine structure of the tongue was mapped by fixing $\Omega$ at some appropriate value and altering a/D over a small range during a time scale of approximately one minute to avoid transient effects by slowly varying the magnetic field strength. Both decaying and increasing amplitude time traces were used; no hysteresis effects were found. Figure 7 shows several power spectra at various a/D and constant $\Omega$ during this procedure. Figure 7a shows the natural shedding frequency with no cylinder oscillation present. In figs. 7b, c and d the cylinder oscillation frequency $f_e$ is shown. We note that there is no shift in the cylinder oscillation frequency as a/D varies, thus confirming our earlier assertions concerning interaction between the two oscillators. We wish to highlight the dramatic changes in the power spectra as a/D is varied. We see three different lock-in tongues, p/q = 4/15, 3/11 and 2/7, all characterized by equally spaced dominant spectral peaks which vary in number from spectra to spectra. These two facts will become important in our determination of the appropriate p/q locked state associated with a particular spectra. However, we interrupt this discussion briefly, and first present fig. 8 documenting the variation in power spectra along the cylinder span when at a fixed $\Omega$ and a/D within a locked-in tongue. Here we choose the 3/10 tongue with $\Omega$ = 0.315 and a/D = 1.2. Two spectra, 100 cylinder diameters apart along the span (each 50 diameters on either side of the tunnel centerline) are presented. We note the similarity between the spectra, both showing equally spaced peaks suggesting a locked-in state. This spanwise correlation is not surprising as it is well known that cylinder oscillations tend to correlate the wake structure along its span, but we felt experimental confirmation of this fact was important to eliminate questions of three dimensional effects from consideration as a possible cause of mode-locking and chaos discussed here.

Let us now return to a discussion of the determination of the appropriate p/q locked state corresponding to a power spectra by introducing fig. 9, which shows two power spectra at the boundary of the 2/7 locked tongue. Figure 9a is a quasiperiodic state while fig. 9b represents a mode-locked state. A mode-locked state is characterized by a power spectrum with equally spaced dominant spectral peaks. The spectral peaks not labeled $f_e$ or $f_o'$ in fig. 9b are simply the sum and difference peaks ($mf_e + nf_o'$) of these two frequencies. Since $f_e/f_o' = p/q$ is a rational number, these difference peaks must be equally spaced. Thus every peak is an integer multiple of $f_e/p$ or $f_o'/q$. Also, the number of dominant spectral peaks with frequency less than or equal to $f_e$ gives us p in the rational ratio p/q. In the quasiperiodic case of fig. 9a, the equal spacing of the peaks is lost. This is expected since $\omega$ is irrational and the difference frequencies are not all integer values, thus we see side peaks surrounding the dominant spectral peaks in the spectrum. The value of q cannot be unambiguously obtained solely from the power spectrum; to do this, one requires a Poincare section or time trace of the system.

It was noted earlier that a Poincare section will contain q discrete points for a p/q locked state. In our experiments we found the creation of Poincare sections to be difficult over long time scales due to the high oscillation frequencies and inherent noise of the system. One creates a Poincare section by sampling the time trace at either of the two dominant frequencies $f_e$ or $f_o'$. This has been accomplished in other fluid systems such as the low aspect ratio Rayleigh-Benard convection cell where typical frequencies are 3 orders of magnitude lower than in our system leading to much longer oscillation time periods. This makes sampling at a fixed frequency inherently easier. In the present system it is difficult to sample exactly at the appropriate frequency, because each period is never exactly an integer multiple of the sampling frequency. This leads to a less distinct demarcation between the Poincare sections of a locked and quasiperiodic states than we have seen in power spectra. For this reason, we turn instead to time traces of the system to determine q. In fig. 10 we show velocity time traces from four different locked-in states. On each of them, the time periods $T_e = 1/f_e$ and $T_o' = 1/f_o'$ are shown. A physical definition of a p/q locked state in the present system is that the cylinder goes through p oscillation cycles while the coupled wake makes exactly q cycles. For example, in the 2/5 locked case in fig. 10 we see that the repeating structure consists of five cycles suggesting that q = 5, and that $2T_e = 5T_o'$, or $\omega = 2/5$. Thus we can determine p/q locked states without resorting to a Poincare section. We note that the difficulties mentioned above in obtaining Poincare sections pertain to sampling over long time scales, and sampling over short time scales yields q distinct points as can easily be seen by studying the 2/5 locked time trace in fig. 10 where the dots represent points sampled at $f_o'$. We see that every fifth point repeats the identical velocity magnitude level over short time scales.

## 5.2 Critical Line Behavior

The experimentally determined devil's staircase along the critical line is shown in figure 11 and compared to the theoretical predictions at K = 1. The symbols represent the limits of the experimental steps while the solid lines represent theoretical predictions. While agreement is not exact, the staircase structure is definitely obtained in experiment. The inset enlarges the boxed region showing the limitation of the agreement between the measured fine structure and that of the devil's staircase. It must be remembered in interpreting these departures that they are of the same order of magnitude as the uncertainty in flow parameters.

In fig. 12 we study the transition to chaos through the golden mean by observing power spectra at a/D below, near, and above the experimentally determined critical line. In fig. 12a we notice a low background turbulence level and no evidence of the self-similiar structure. Near the critical line the background broadband fluctuation level has risen, and additional peaks appear forming the self similiar structure predicted by circle maps. At higher a/D above the critical line we note a further increase in background turbulence level, but the peaks no longer appear self-similar, and the banded structure is partially lost. In fig. 13 we present the wake velocity time trace at the best approximation to the critical golden mean point we have been able to attain, with its scaled power spectrum presented in fig. 14. The dressed winding number $\omega$ is within 0.1% of $\sigma_G$. This spectrum is averaged over approximately 65000 cycles of the cylinder oscillation frequency. In fig. 14 the principal peaks fall at powers of $\sigma_G$ down to $\sigma_G^5$. They are nearly of constant amplitude except for $\sigma_G^5$ which falls off. We note the generation 2 and 3 peaks fall as predicted by the mixing coefficients within the resolution of our power spectrum. We also see peaks from generations 2 and 3 with generation 2 peaks showing the constant amplitude trend (within 0.5 dB), but the behavior degrades for generation 3 peaks. Generation 2 and 3 peaks are not present at lower frequencies and higher order generations are not observed at all. Some of these departures from universality occur no doubt because $\omega$ could not be maintained to better than 0.1% of $\sigma_G$.

From velocity time traces such as presented in fig. 13 we obtained Poincare sections for the critical golden mean point. We have previously noted our difficulties in obtaining Poincare sections by sampling the continuous time trace at time steps separated by the period of forcing. As a result we utilized a slightly modified method in which we sampled at extremum (minima) in the velocity time trace, obtaining, say, u(1), u(2), u(3), u(4),... and embedded these points in three dimensions, the lowest dimension in which the attractor was non-intersecting, by plotting u(n) *vs* u(n+1) *vs* u(n+2). These sampled points were on the average separated by the period of forcing. This procedure led to attractors which were much less "noisy" than using the standard technique. Our motivation for this method lies in studies of computer-generated two-frequency quasiperiodic time traces in which the above procedure yields an attractor topologically equivalent to a circle as expected. Also, a three-frequency quasiperiodicity time trace yields a two-torus. We note that the above embedding scheme satisfies $d \geq 2N+1$ as the attractor is topologically equivalent to a limit cycle with one degree of freedom, hence N=1.

## 5.3 Generalized Dimensions and the Singularity Spectrum

We next divide the Poincare section into equal boxes of length r and determine the slopes in the plots of $\log(\Gamma(r,q))/(q-1)$ *vs* $\log r$. This gives us $D_q$. Figure 15 shows typical plots for q=2 and q=–2. We see that the linearity of the plot is excellent over two decades. The noise level on the attractor is indicated on the figure and we see that for q=-2 (more rarefied) the linearity degrades much more below the noise level than in the q=2 (more concentrated) case. This corresponds with our observation that the rarefied regions on the original attractor appear noisier. It is to be expected that more error in the $D_q$ *vs* q curve would occur for $q < 0$. In fig. 16 the experimental data are shown with the solid line representing the theoretical prediction. The experimental data presented is the average of Poincare sections representing our best three approximations to the critical golden mean point all with dressed winding number within 0.1% of the golden mean. The limited nature of this data reflects the difficulty in maintaining the dressed winding number to such a close approximation to the golden mean as well as the degradation in the Poincare sections obtained as one moves away from the critical point. We see good agreement between experiment and theory especially for $q > 0$ and also the expected degradation for $q < 0$. Typical error bars on the data are also shown, representing variations between different realizations and uncertainties in determining the linear slope from the log-log plots. In fig. 17 we present the $f(\alpha)$ *vs* $\alpha$ curve derived from fig. 16 showing data points for the three individual cases. Again the general similarities and small departures from the theoretical are obvious. The right side of the curve (larger $\alpha$) corresponds to the more rarefied regions on the Poincare section and again the expected degradation is noted.

We are now in a position to calculate one of the scaling coefficients discussed in Section 2 namely $\alpha_{GM} = 1.28857...$ which, for the circle map, determines the scaling of iterates around $\theta=0$. A general property of the $f(\alpha)$ *vs* $\alpha$ curve is that $\alpha_{min} = D_\infty$, while $\alpha_{max} = D_{-\infty}$. For the sine circle map [23], $D_{-\infty} = 1.8980$ and $D_\infty = 0.6326$. To calculate them, we iterate the circle map and truncate at some iterate given by some large number in the Fibonacci sequence, say $F_{17} = 2584$. To determine the $D_q$'s we assign equal probability to each iterate so that $p_i = 1/2584$ and study the distances between iterates which are unequally spaced. In the most rarified portions of the map near $\theta=0$, the iterates scale as $r \sim \alpha_{GM}^{-n}$, and $p_i \sim 1/F_n \sim (\sigma_G)^n$. This leads to $D_{-\infty} = \ln(\sigma_G)/\ln(\alpha_{GM}^{-1}) = 1.8980...$ Similarly, $D_\infty = \ln(\sigma_G)/\ln(\alpha_{GM}^{-3}) = 0.6326...$, due to the cubic inflection point at $\theta=0$. Thus, from the experimental $\alpha_{min} = 0.67$ and $\alpha_{max} = 1.75$, we can obtain two estimates for $\alpha_{GM}$. We obtain $\alpha_{GM} = 1.27$ and 1.317 using $\alpha_{min}$ and $\alpha_{max}$ respectively, which are both within 3% of the value appropriate to the circle map.

Note that with the present experimental accuracies we are unable to determine

the other scaling parameter $\delta$ (defined in Section 2) as this requires obtaining the widths of mode locked tongues around the critical golden point to very fine resolution. At present we have been able to resolve these widths only up to the 8/13 tongue.

## 6. CONCLUSIONS

Even though some departures from the universality associated with the circle map behavior exist in the flow behind a circular cylinder, we think that the extent of observed similarity is remarkable. It is not obvious whether the departures are real, or occur because the control of experimental parameters was not as fine-tuned as desired. It is known, however, that very small departures from criticality can produce similar behavior. As already noted, inherent difficulties in establishing a wind tunnel flow with extremely fine control made it impossible to control $\sigma_G$ to better than 0.1%. The departures observed in the devil's staircase construction are of the same order of magnitude as the uncertainties in the flow parameters. Further, largest departures in the $f(\alpha)$ curve occur for large $\alpha$ consistent with the relatively large influence of noise on the most rarified regions of the Poincare section. *Apropos* of this somewhat unsatisfactory state of affairs, we reiterate that enormous care was exercised in the experiments, and state our belief that the residual problems of fine control cannot be eliminated without resorting to unconventional ways of generating such flows; some thoughts on this are currently being investigated.

It remains for us to comment on the meaning of the word 'universal' given that we had to exercise exquisite control on flow parameters to observe the behavior that we did; in fact, as we have already remarked, approaching the golden mean by as close as 0.1% was not enough to observe all aspects of 'universality'. It is often implied that this type of 'universality', occurring in a 'zero measure volume' of parameter space, is of no great significance to the physics of the problem. This, however, is not the meaning of 'universality'. It is to be interpreted to mean the behavior which is common to a broad class of physical systems independent of the dynamical equation governing the system dynamics. To know that circle maps predict quantitatively something of wakes is quite astounding!

Although we have experimentally demonstrated that the wake of an oscillating cylinder behaves similar to a circle map in many respects, we have not yet shown that circle map can be extracted from the Navier-Stokes equations in the proper approximation. Work in this direction, although unfinished, seems promising.

## ACKNOWLEDGMENTS

We acknowledge useful discussions with C. Meneveau and A. Chhabra. The research was supported by a grant from the Air Force Office of Scientific Research and a University Research Initiative Grant from the Defence Advanced Research Projects Agency.

## REFERENCES


1. Landau, L.D. and Lifshitz, E.M., Fluid Mechanics (Volume 6 of the Course of Theoretical Physics), Pergamon Press, 1982, pp. 103-107.

2. Feigenbaum, M.J., "Quantitative Universality for a Class of Nonlinear Transformations", Journal of Statistical Physics, Vol. 19, No. 1, 1978, pp. 25-52.

3. Feigenbaum, M.J., "The Onset Spectrum of Turbulence", Physics Letters, Vol. 74, No. 6, Dec. 1979, pp. 375-378.

4. Shenker, S.J., "Scaling Behavior in a Map of a Circle onto Itself: Empirical Results", Physica D, Vol. 5, 1982, pp. 405-411.

5. Feigenbaum, M.J., Kadanoff, L.P., and Shenker, S.J., "Quasiperiodicity in Dissipative Systems: A Renormalization Group Analysis", Physica D, Vol. 5, 1982, pp. 370-386 .

6. Ostlund, S., Rand, D., Sethna, J., and Siggia, E., "Universal Properties of the Transition from Quasiperiodicity to Chaos in Dissipative Systems", Physica D, Vol. 8, 1983, pp. 303-342.

7. Rand, D., Ostlund, S., Sethna, J., and Siggia, E., "Universal Transition from Quasiperiodicity to Chaos in Dissipative Systems", Physical Review Letters, Vol. 40, No. 2, July 1982, pp. 132-135.

8. Ruelle, D., and Takens, F., "On the Nature of Turbulence", Commun. Math. Phys. , Vol. 20, 1971, pp. 167-192.

9. Newhouse, S., Ruelle, D., and Takens, F., "Occurrence of Strange Axiom A Attractors Near Quasi Periodic Flows on $T^m$, m>3", Commun. Math. Phys., Vol. 64, 1978, pp. 35-40.

10. Stavans, J., Heslot, F., and Libchaber, A., "Fixed Winding Number and the Quasiperiodic Route to Chaos in a Convective Fluid", Physical Review Letters, Vol. 55, No. 6, Aug. 1985, pp. 596-599.

11. Jensen, M.H., Kadanoff, L.P., Libchaber, A., Procaccia, I., and Stavans, J. "Global Universality at the Onset of Chaos: Results of a Forced Rayleigh-Benard Experiment", Physical Review Letters, Vol. 55, 1985, pp. 2798-2801.

12. Fein, A.P., Heutmaker, M.S., and Gollub, J.P., "Scaling at the Transition from Quasiperiodicity to Chaos in a Hydrodynamic System", Physica Scripta, Vol. T9, 1985, pp. 79-84.

13. Stavans, J., "Experimental Study of Quasiperiodicity in a Hydrodynamical System", Physical Review A , Vol. 35, No. 10, May 1987, pp. 4314-4327.

14. Glazier, J.A., Jensen, M.H., Libacher, A. and Stavans, J., "Structure of Arnold tongues and the f($\alpha$) spectrum for period doubling: Experimental results",

Physical Review A, Vol. 34, No. 2, Aug. 1986, pp. 1621-1624.

15. Glazier, J.A., Gunaratne, F., and Libacher, A., "f(α) Curves: Experimental", Physical Review A , Vol. 37, No. 2, Jan. 1988, pp. 523-530.

16. Sreenivasan, K.R., "Transition and Turbulence in Fluid Flows and Low-Dimensional Chaos", Frontiers of Fluid Mechanics, (eds. Davis S.H. and Lumley J.L.), Springer, 1985, pp. 41-67.

17. Sreenivasan, K.R., and Ramshankar, R., "Transition Intermittency in Open Flows, and Intermittency Routes to Chaos", Physica D, Vol. 23, 1986, pp. 246-258.

18. Sreenivasan, K.R., and Strykowski, P.J., "On analogies between turbulence in open flows and chaotic dynamical systems", Turbulence and Chaotic Phenomena in Fluids, (ed. Tatsumi, T.), North-Holland, 1984, pp. 191-196

19. Schewe, G., "Experimental Observation of the Golden Section in Flow Round a Circular Cylinder", Physics Letters, Vol. 109A, No. 1, May 1985, pp. 47-50.

20. Olinger, D.J., and Sreenivasan, K.R., "Nonlinear Dynamics of the Wake of an Oscillating Cylinder", Physical Review Letters, Vol. 60, No. 9, Feb. 1988, pp. 797-800.

21. Takens, F., In Lecture Notes in Mathematics 898 (eds. Rand, D.A. and Young, L.S.), Springer-Verlag, 1981, p. 366

22. Eckmann, J.P., and Ruelle, D., "Ergodic Theory of Chaos and Strange Attractors", Review of Modern Physics, Vol. 57, 1986, pp. 617-656.

23. Halsey, T.C., Jensen, M.H., Kadanoff, L.P., Procaccia, I., and Shraiman, B.I., "Fractal Measures and Their Singularities: The Characterization of Strange Sets", Physical Review A, Vol. 33, No. 2, Feb. 1986, pp. 1141-1151.

24. Hentschel, H.G.E., and Procaccia, I., "The Infinite Number of Generalized Dimensions of Fractals and Strange Attractors", Physica D, Vol. 8, 1983, pp. 435-444.

25. Mandelbrot, B., "Intermittent Turbulence in Self-Similar Cascades: Divergence of High Moments and Dimension of the Carrier", Journal of Fluid Mechanics, Vol. 62, 1974, pp. 331-358.

26. Jensen, M.H., Bak, P., and Bohr, T., "Transition to Chaos by Interaction of Resonances in Dissipative Systems. I. Circle Maps", Physical Review A, Vol. 30, No. 4, Oct. 1984, pp. 1960-1969.

27. Sreenivasan, K.R., Strykowski, P.J., and Olinger, D.J., "Hopf bifurcation, Landau equation, and vortex shedding behind circular cylinders", ASME forum on unsteady flow separation, vol. 52 of the Fluids Engineering Division (ed. K.N. Ghia), 1987, pp. 1-13.

28. Van Atta, C.W., and Gharib, M., "Ordered and Chaotic Vortex Streets Behind Circular Cylinders at Low Reynolds Numbers", Journal of Fluid Mechanics, Vol. 174, 1987, pp. 113-133.

29. Koopman, G.H., "The Vortex Wakes of Vibrating Cylinders at Low Reynolds Numbers", Journal of Fluid Mechanics, Vol. 28, 1967, pp. 501-512.

30. Stansby, P.K., "The Locking-On of vortex Shedding due to the Cross-Stream Vibration of Circular Cylinder in Uniform and Shear Flows", Journal of Fluid Mechanics, Vol. 74, 1976, pp. 641-665.

31. Ongoren, A., and Rockwell, D., "Flow Structure from an Oscillating Cylinder Part 1. Mechanisms of Phase Shift and Recovery in the Near Wake", (to appear in Journal of Fluid Mechanics), 1988.

32. Bearman, P.W., "Vortex Shedding from Oscillating Bluff Bodies", Annual Review of Fluid Mechanics, Vol. 16, 1984, pp. 195-222.

33. Berger, E., and Wille, R., "Periodic Flow Phenomena", Annual Review of Fluid Mechanics, Vol. 4, 1972, pp. 313-340.

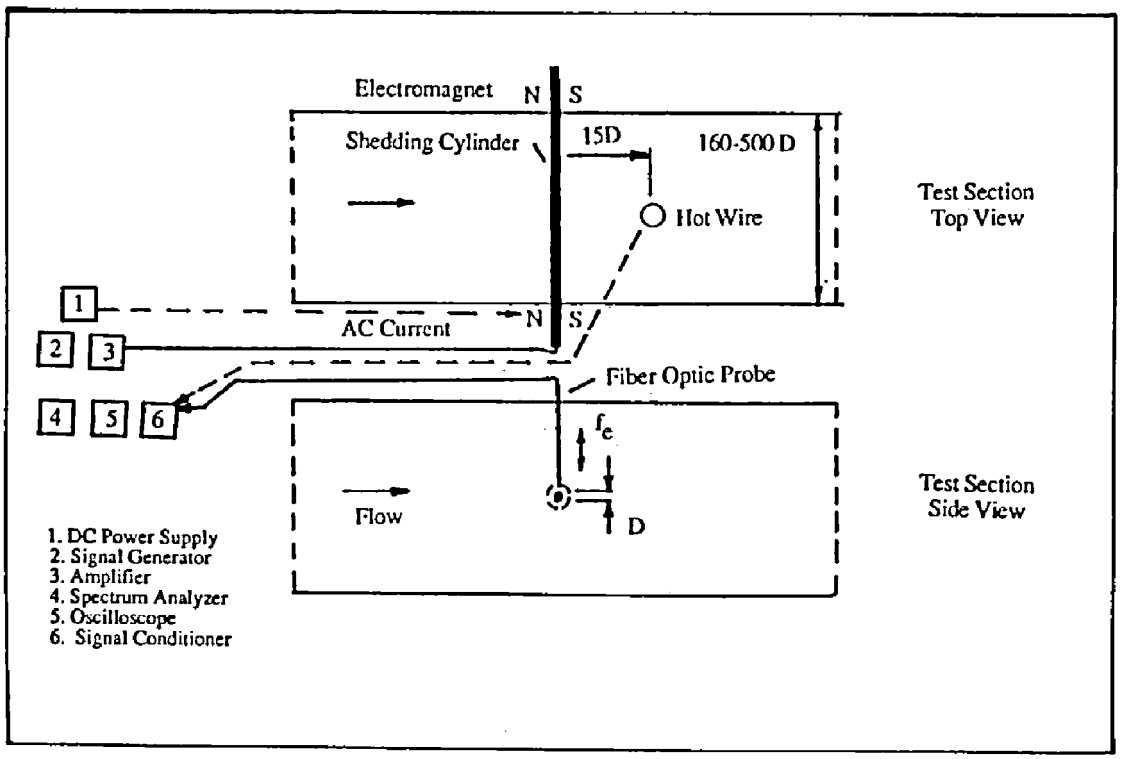


Figure 1: Detailed schematic of the experimental set-up.

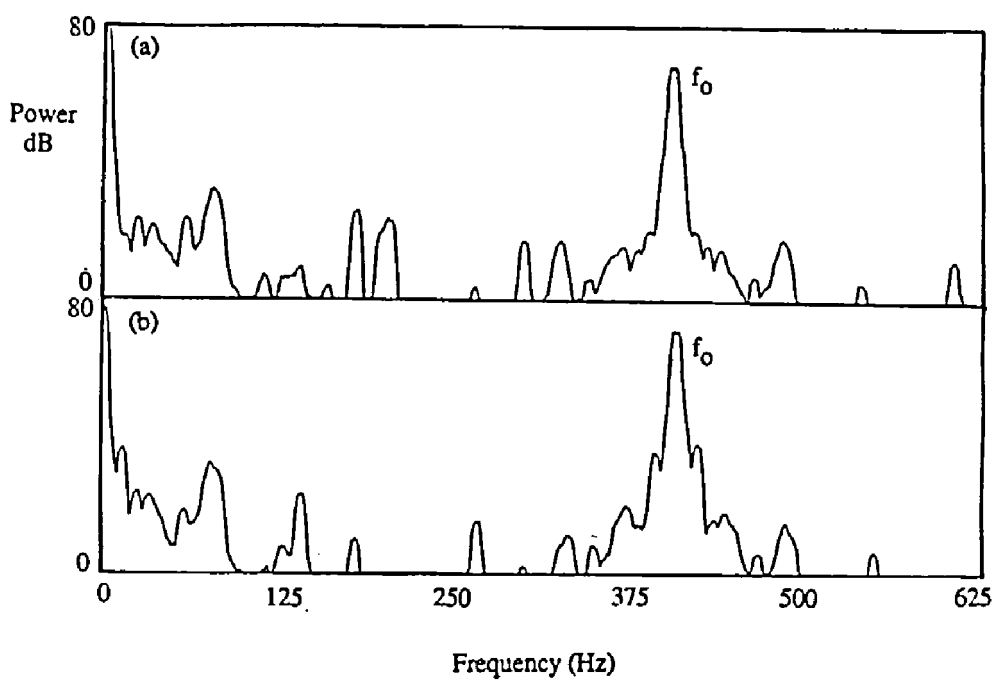


Figure 2: Power spectral density for the case of natural vortex shedding; (a) with cylinder current on, $f_o$ = 404.9 Hz ; (b) with cylinder current off, $f_o$ = 407.0 Hz.

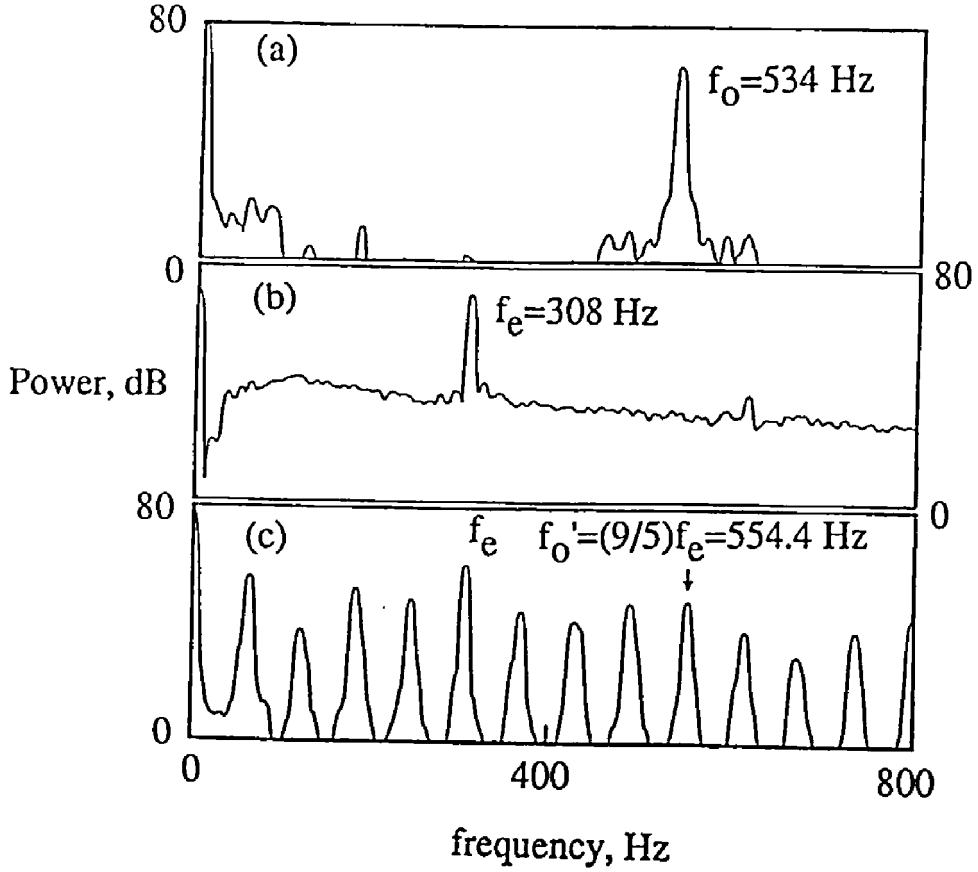


Figure 3: (a) Power spectral density of the hot wire wake velocity signal for natural vortex shedding at $f_o$ = 534.0 Hz. (b) The corresponding data for the oscillating cylinder, measured with the fiber optic probe; $f_e$ = 308.0 Hz. In (c), frequency locking occurring due to excitation is seen. The natural shedding frequency disappears in favor of the new peak at 9/5 $f_e$; peaks appear at other fractions of $f_e$.

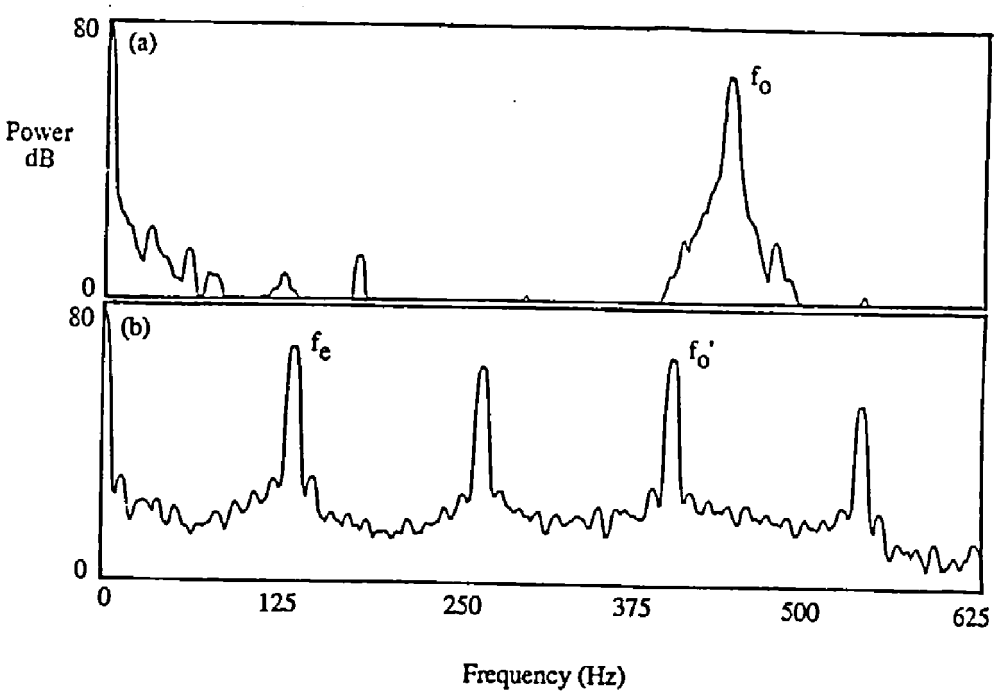


Figure 4: Power spectral densities for a 1/3 lock-in case: (a) Natural vortex shedding at $f_o$= 443.75 Hz; (b) Coupled vortex wake at $f_o'$= 403.13 Hz; $f_e$=134.38 Hz.

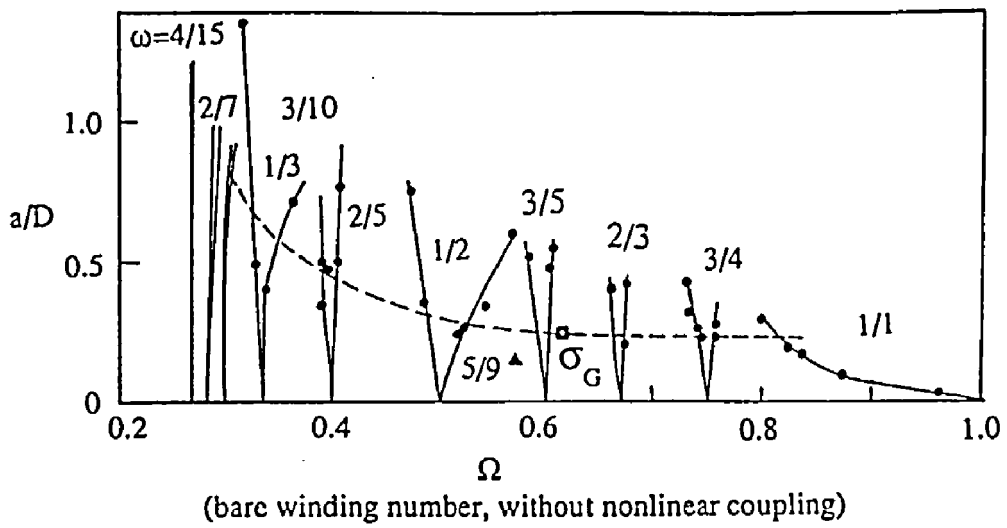


Figure 5: Arnold tongues (that is, the locked-in regions) in the wake of the oscillating cylinder. The ordinate is the amplitude of oscillation normalized by the cylinder diameter. About 30 such tongues were noted, but only those with reasonable width are shown. In each tongue, the natural shedding frequency disappears in favor of a rational p/q multiple of the excitation frequency, and the appropriate multiplication factor is shown in each tongue. The critical line (corresponding to the K=1 line in the circle map), as determined by the onset of chaos is shown dashed.

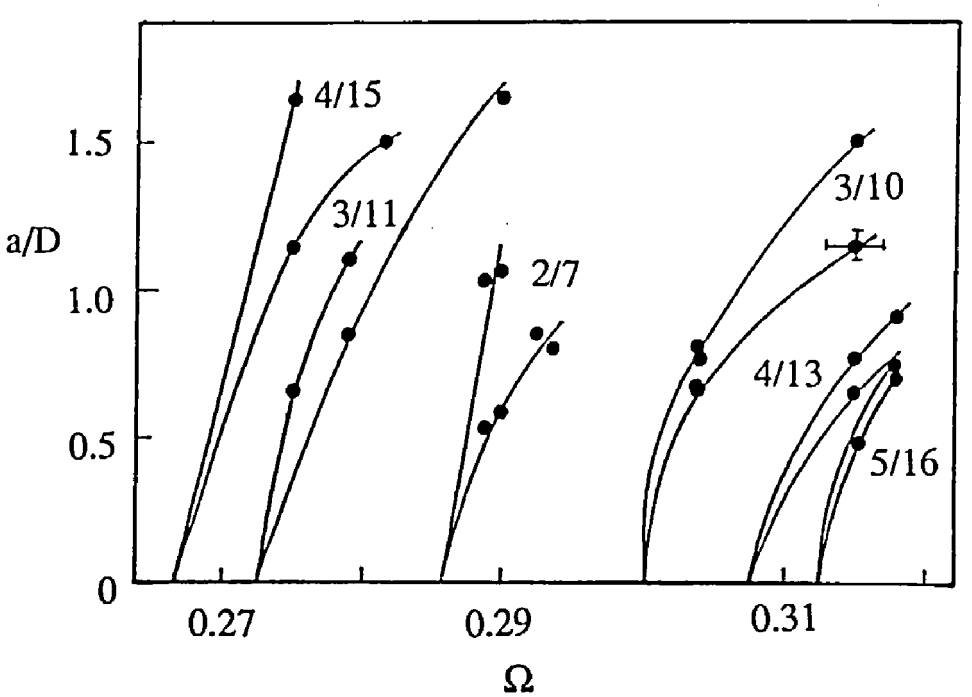


Figure 6: The fine structure in a small region of the a/D-Ω plane of fig. 5. Typical experimental uncertainties are shown.

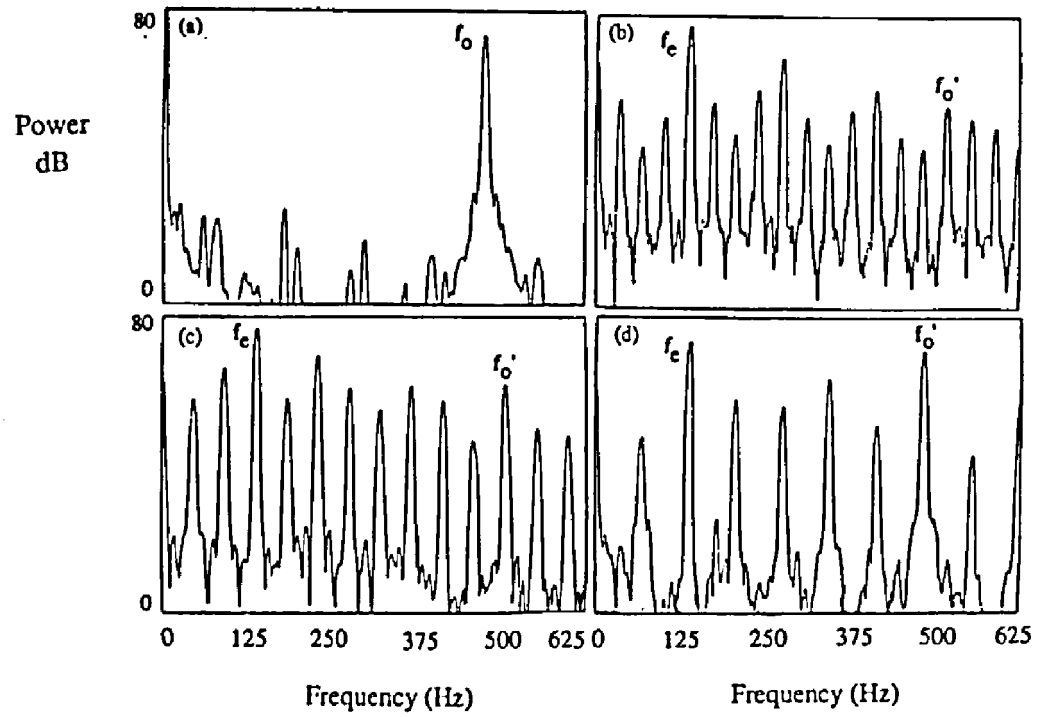


Figure 7: Power spectral densities mapping the fine structure of the a/D-Ω plane at a fixed Ω=0.29, $f_e$ = 139.0 Hz, $f_o$=479.7 Hz; (a) Natural vortex shedding at $f_o$; (b) 4/15 lock-in case, $f_o'$ = 521.25 Hz, a/D = 1.75; (c) 3/11 lock-in case, $f_o'$=509.6 Hz, a/D=1.6; (d) 2/7 lock-in case, $f_o'$=486.5 Hz, a/D = 0.9.

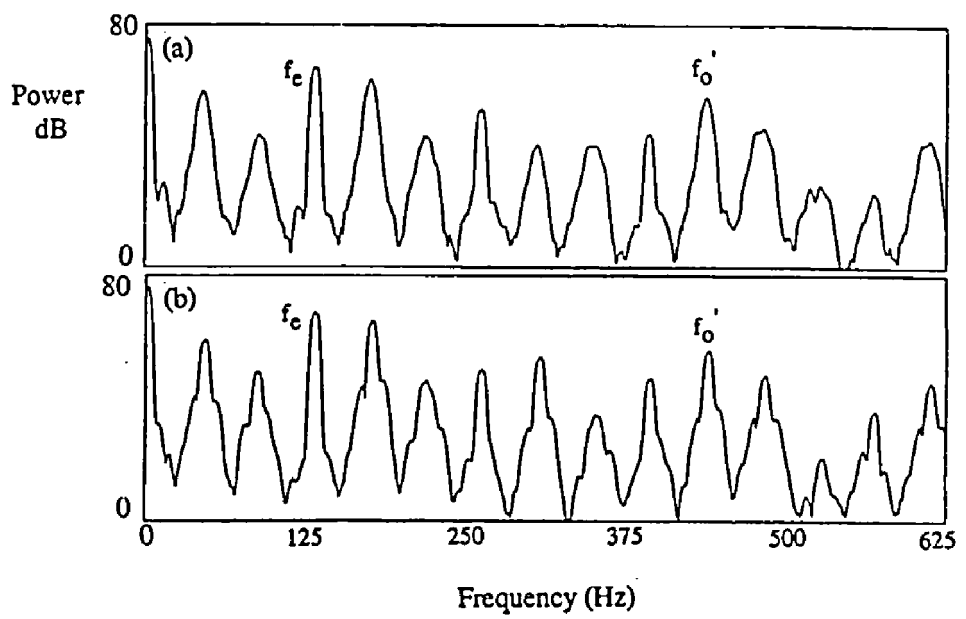


Figure 8: Variation in power spectra in spanwise direction along cylinder span within the 3/10 lock-in tongue; (a) and (b) represent two spectra spaced 100 cylinder diameters apart, both 50 diameters from tunnel centerline. Ω = 0.315 , a/D = 1.2, $f_e$= 131.25 Hz, $f_o$ = 415.63 Hz, and $f_o'$ = 437.5 Hz.

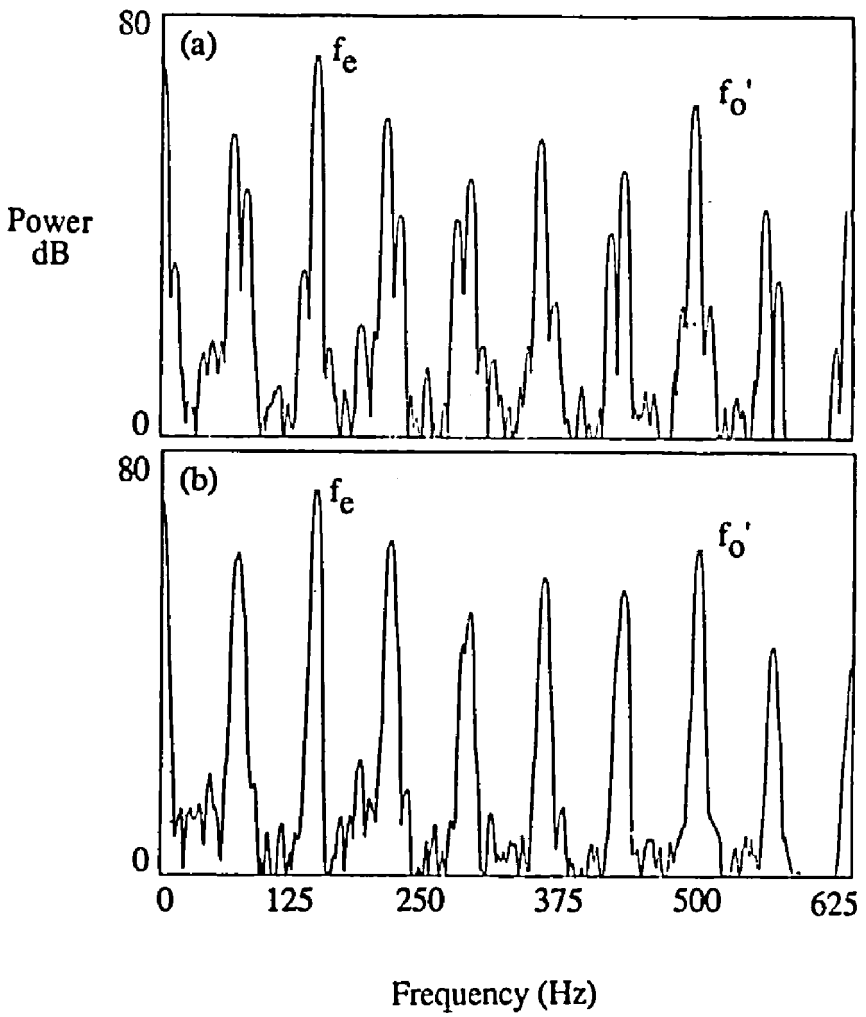


Figure 9: Power spectral densities at boundary of 2/7 lock-in tongue. (a) Quasiperiodic state, $f_o'$= 482.8 Hz, a/D = 0.5; (b) Lock-in state $f_o'$ = 486.5 Hz, a/D = 0.75; Cylinder oscillation frequency, $f_e$ =139.0 Hz, $f_o$= 473.4 Hz.

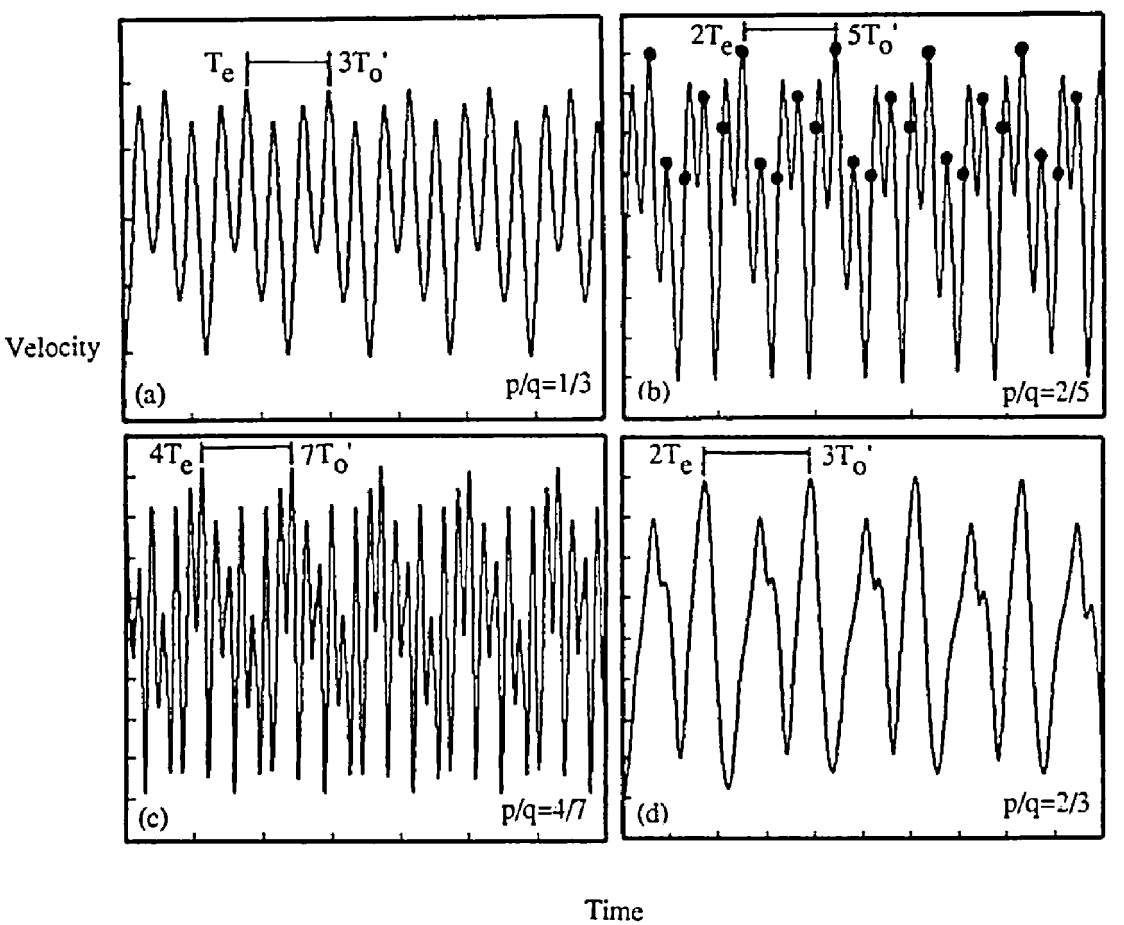


Figure 10: Hot wire velocity time traces from coupled cylinder wake with oscillation present showing various p/q lock-in states. (a) 1/3 lock-in, (b) 2/5 lock-in, (c) 4/7 lock-in, and (d) 2/3 lock-in. Cylinder oscillation period $T_e$ and coupled wake oscillation period $T_o'$ are shown. Symbols (●) in (b) represent discrete points separated by the coupled wake oscillation period $T_o'$.

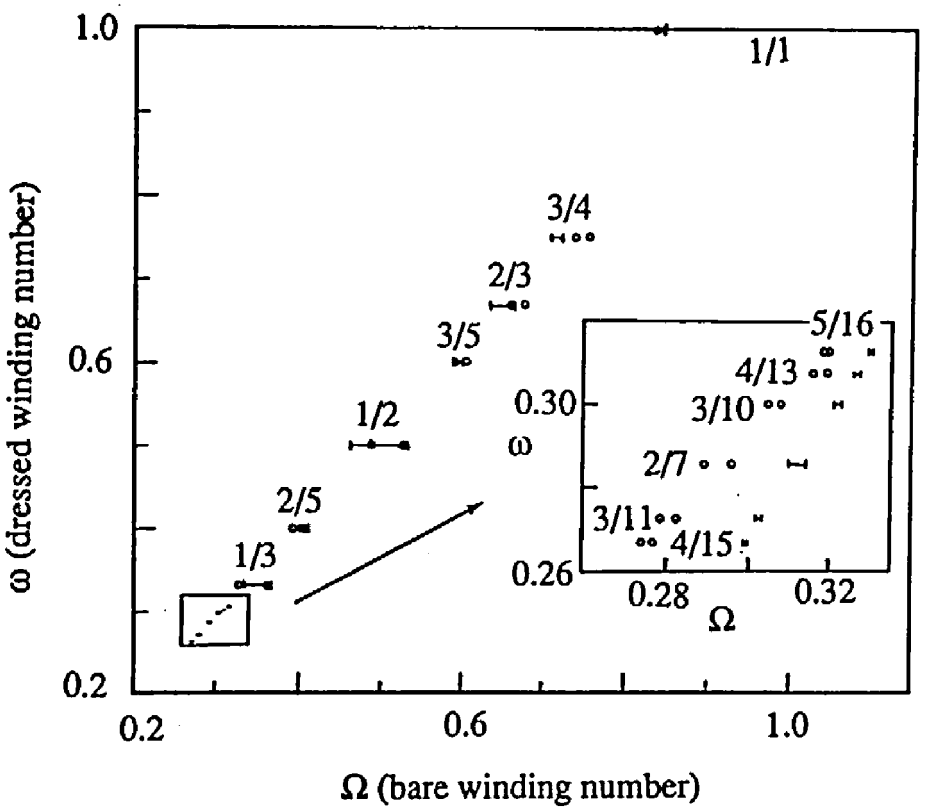


Figure 11: The devil's staircase structure using the data of figs. 5 and 6 along the experimentally determined critical line. Although the general pattern is the same as for the circle map, there are some noticeable departures.

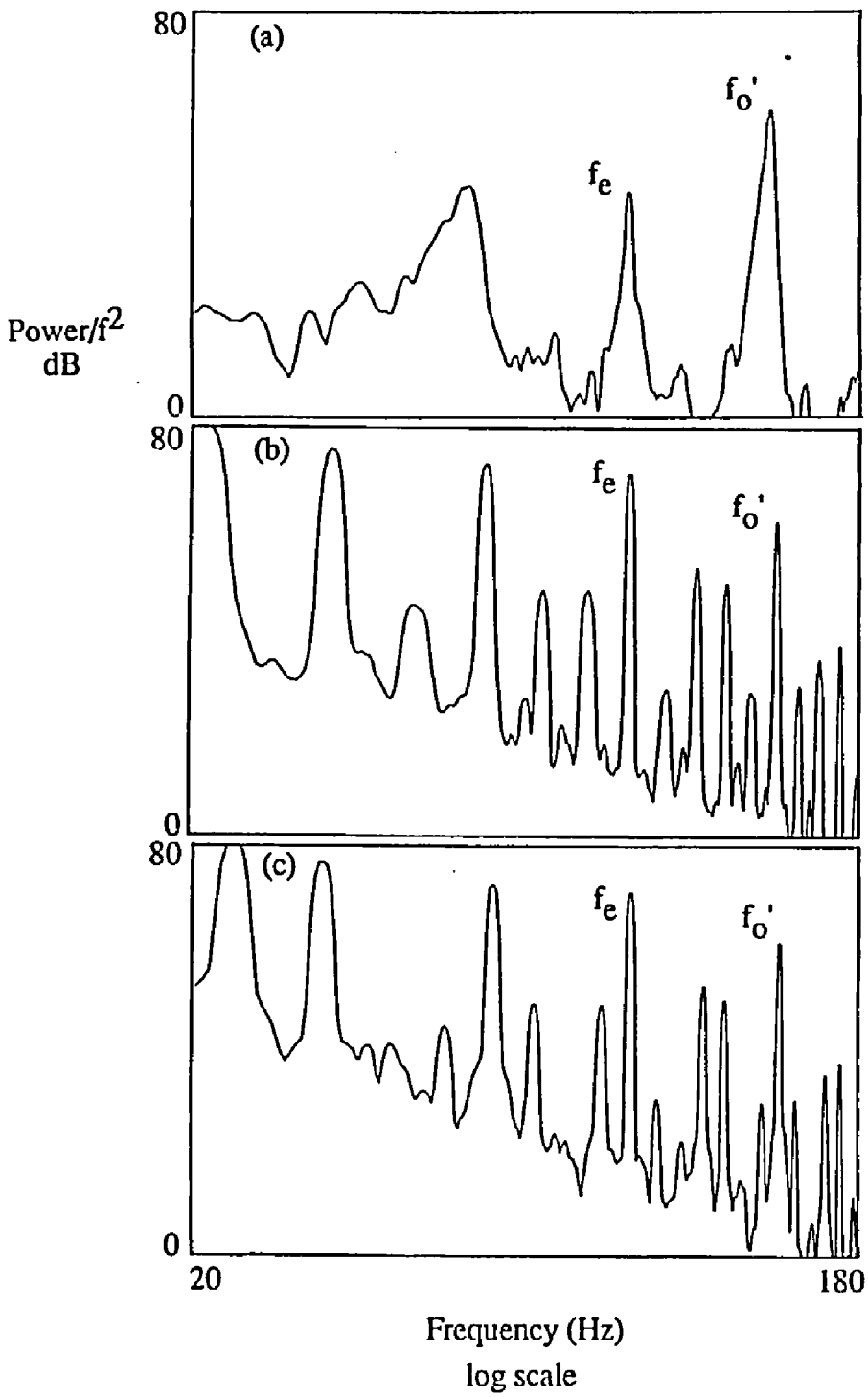


Figure 12: Scaled power spectra at dressed winding number $\omega = \sigma_G$ showing transition to chaos through critical golden mean. (a) below critical line, a/D = 0.06; (b) near critical line, a/D = 0.22; and (c) above critical line, a/D = 0.33. Here $f_e$ = 84.4 Hz, and $f_o'$ = 136.5 Hz.

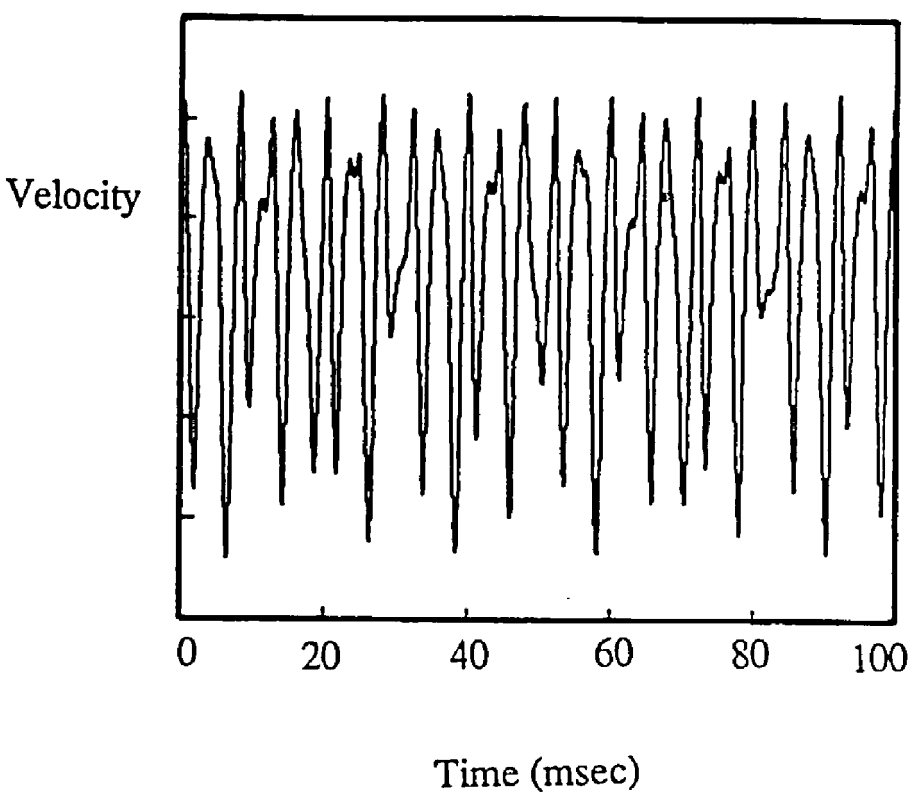


Figure 13: Hot wire wake velocity time trace at the nearest approximation to critical golden mean point (dressed winding number to within 0.1 % of $\sigma_G$).

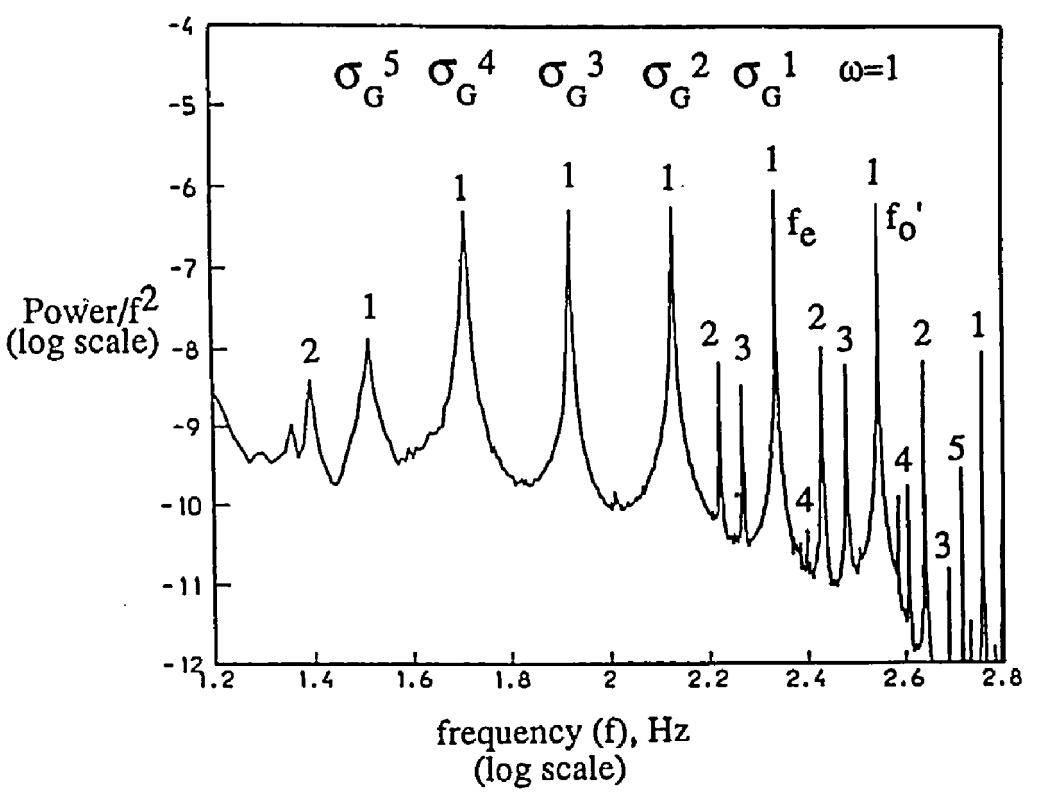


Figure 14: Frequency scaled power spectrum for the excited wake at the critical golden mean point.

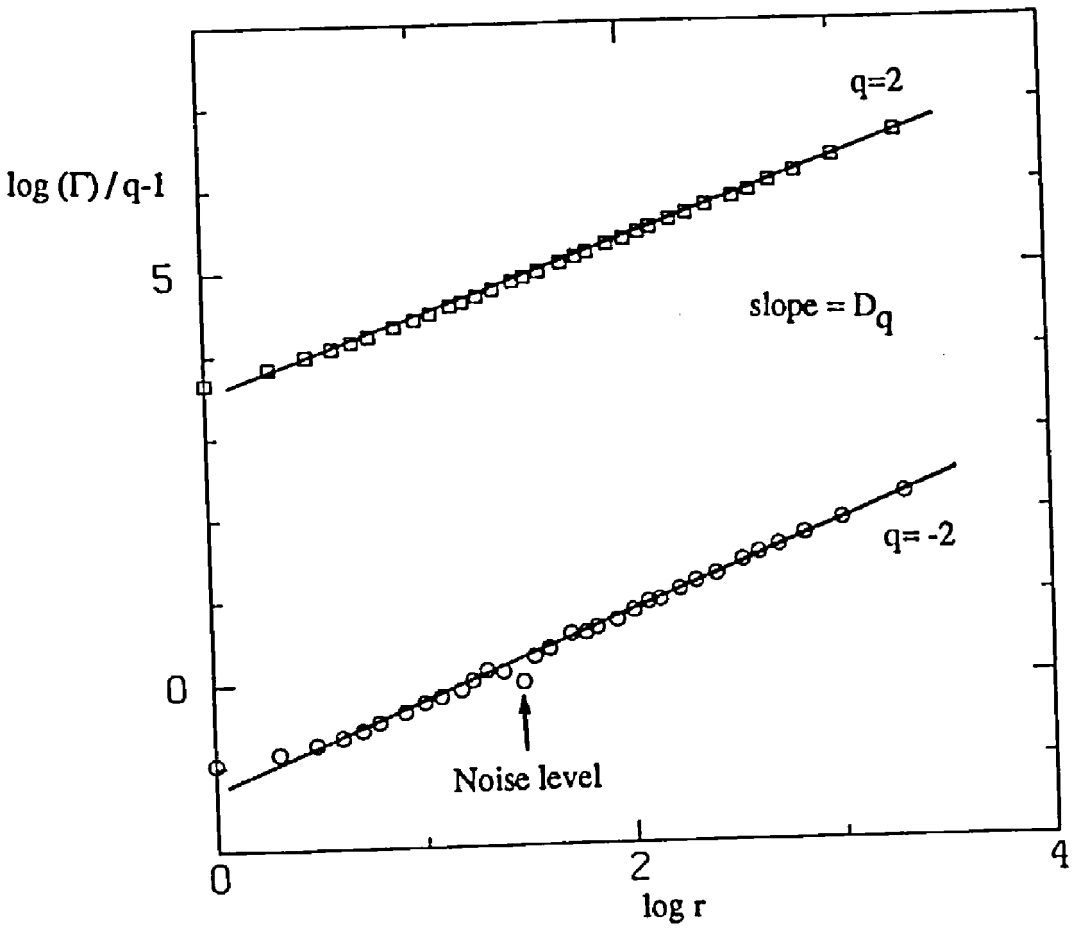


Figure 15: Scaling of the probability moments for two different q's from the experimental Poincare section . Good linearity over approximately two decades is noted.

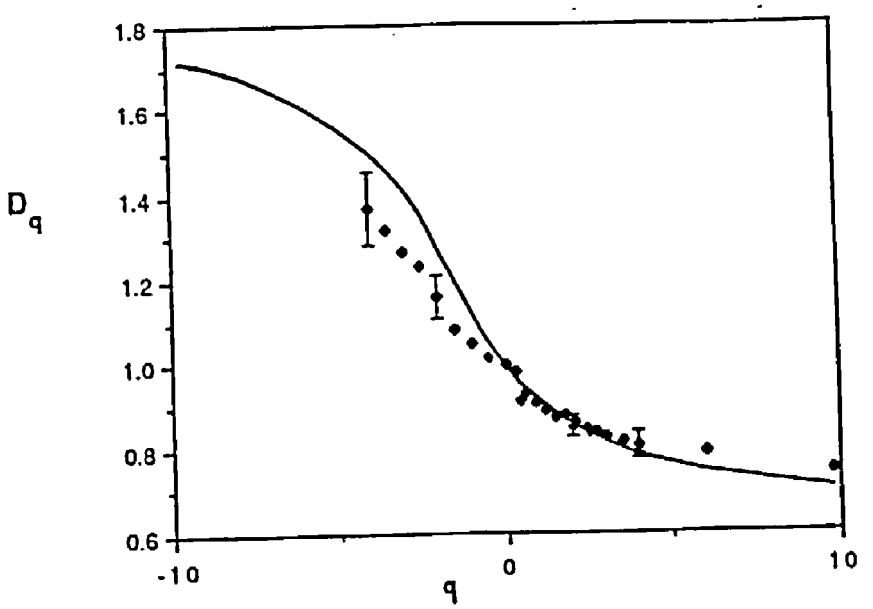


Figure 16: The generalized dimensions, $D_q$ *vs* q curve derived from fig. 15 for q between −5 and 10. Typical uncertainties are shown by error bars.

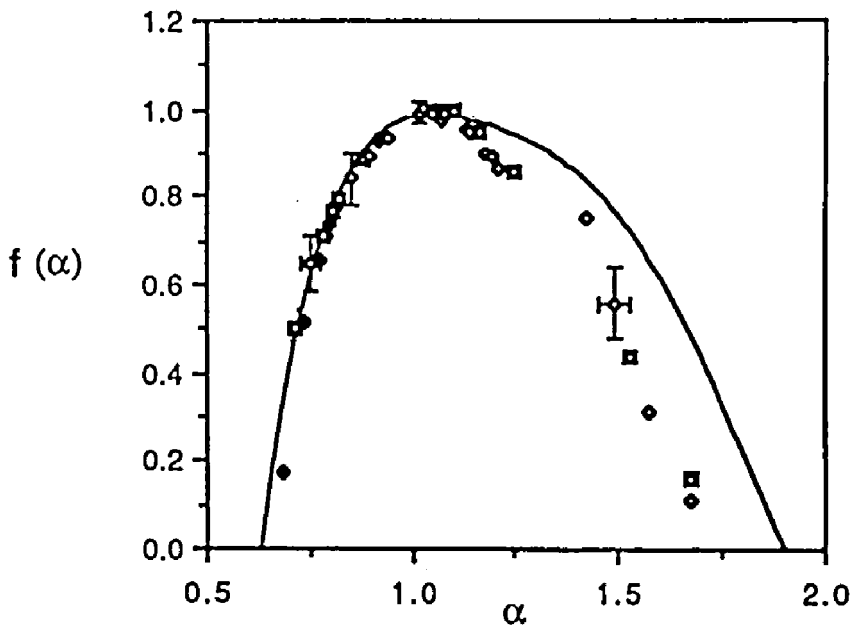


Figure 17: The f(α) curve obtained *via* Legendre transform of the measured generalized dimensions. Levels of uncertainty are shown by error bars.